Effects of confinement on anomalies and phase transitions of core-softened fluids

Leandro B. Krott,[1,*] José Rafael Bordin,[2,†] Ney Marçal Barraz Jr,[3,‡] and Marcia C. Barbosa[1,§]

[1] *Instituto de Física, Universidade Federal do Rio Grande do Sul, Caixa Postal 15051, CEP 91501-970, Porto Alegre, RS, Brazil*

[2] *Campus Caçapava do Sul, Universidade Federal do Pampa, Av. Pedro Anunciação, s/n, CEP 96570-000, Caçapava do Sul, RS, Brazil*

[3] *Campus Cerro Largo, Universidade Federal da Fronteira Sul, Av. Jacob Reinaldo Haupenthal, 1580. CEP 97900-000, Cerro Largo, RS, Brazil*

(Dated: March 18, 2015)

Abstract

We use Molecular Dynamics simulations to study how the confinement affects the dynamic, thermodynamic and structural properties of a confined anomalous fluid. The fluid is modeled using an effective pair potential derived from the ST4 atomistic model for water. This system exhibits density, structural and dynamical anomalies and the vapor-liquid and liquid-liquid critical points similar to the quantities observed in bulk water. The confinement is modeled both by smooth and structured walls. The temperatures of extreme density and diffusion for the confined fluid show a shift to lower values while the pressures move to higher amounts for both smooth and structured confinement. In the case of smooth walls, the critical points and the limit between fluid and amorphous phases show a non-monotonic change in the temperatures and pressures when the the nanopore size is increase. In the case of structured walls the pressures and temperatures of the critical points varies monotonically with the pore size. Our results are explained on basis of the competition between the different length scales of the fluid and the wall-fluid interaction.

PACS numbers: 64.70.Pf, 82.70.Dd, 83.10.Rs, 61.20.Ja

I. INTRODUCTION

Water is an important material in industry, technology and biological processes due to its unusual properties. Water unusual properties comprise many anomalous behavior, with 70 known anomalies[1], like the maximum value of its density in $T = 4^o$C at room pressure, and the increase of the diffusion as the system is compressed[2–4]. These anomalies have been explained in terms of the formation of hydrogen bond network. The water molecules form open and compact (bonded and non-bonded) clusters of tetramers. From the competition between these structures the anomalies arise.

As a natural consequence of the polymorphism of water clusters the pressure-temperature phase diagram of water is very complex. At low temperatures, water shows a coexistence of two amorphous phases: a low density amorphous and a high density amorphous. For higher temperatures, these two amorphous phases might lead to the appearance of two liquid phases, separated by a first order phase transition line ended in a liquid-liquid critical point ($LLCP$). Whereas, homogeneous nucleation occurs in this region, that is called *no man's land*, and because of that, it is an incredible hard task to do experimental measures of liquid water in bulk systems in this region. Theoretically, the existence of these two liquid phases was evidenced in the atomistic ST4 model by Poole and co-authors[5] and confirmed in recent simulations[6,7]. As well, new experiments suggests the coexistence of a high-density and low-density liquid phase of water[8]. A $LLCP$ was also predicted for others atomistic models of water[9–14], and in models for phosphorus[15], silica[16,17], silicon[18], carbon[19], hydrogen[20] and colloidal systems[21]. On the other hand, recent studies suggests that the $LLCP$ can be an open trend on supercooled water and other materials.[22–24]. In this way, there is still several open questions about the $LLCP$.

As an attempt to avoid the crystallization of water in the *no man's land*, experiments with nanoconfined water have been performed recently[25–27]. The presence of a confining structure changes the number of hydrogen bonds, avoiding the nucleation. Some experiments of water confined in nanopores, performed by x-ray and neutron scattering, show that liquid states persist down to temperatures much lower than in bulk[28–30]. The nanopores size has important influence in the crystallization of the system[28,30–33], and hydrophilic and hydrophobic nanopores can lead to distinct results as well[29,34].

Classical atomistic models for water are important tools to understand its properties.

On the other hand, coarse-grained models arise as an interesting tool to see the universal mechanisms that lead to anomalous waterlike properties. Coarse-grained models may reproduce diffusion and density anomalies and can be modeled by core-softened (CS) potentials with two length scales, that can be constructed using a shoulder or a ramp potential[35–40]. These coarse-grained models for anomalous fluids are able to capture the bulk waterlike anomalies and averaged properties in the confined materials. When confined by fixed hydrophilic plates, the fluid-wall interaction can induce solidification and shift the anomalous properties to higher temperatures, while hydrophobic nanopores lead the system to remain in liquid state and shift the waterlike anomalies to lower temperatures in relation to bulk[41,42]. Whereas, when the nanopore has at least one degree of freedom, given by the mobility of the plates in z direction, the anomalous behavior of the fluid disappears and distinct phase transitions are observed[43–46]. CS fluids confined in nanotubes also present interesting findings, similar to obtained in atomistic models for water, as the increase in diffusion coefficient and flux for narrow nanotubes associated to a layer to single-file transition and a discontinuity in the enhancement flow factor[47–49]. The drawback of these core-softened potentials is that due to the simplicity of the two length scales, they are not capable to reproduce the effects related to the third coordination shell of the anomalous fluid what might be relevant under confinement[50].

In addition to the relevance of the detail structure of the liquid, the structure of the confining system is also relevant since biological and physical materials do not exhibit the smoothness and regularity of the flat walls and tubes employed in the simulations. This naturally raises the question of what is the role played by the structure of the liquid and of the interface in the thermodynamic, dynamic and structural behavior of confined systems. Recent simulations have shown that the hydrophobic or hydrophilic behavior of the confining surfaces are governed by the interfacial free energy, that strongly depends on the surface structure[51]. Even thought these simulations do not observe important differences in the diffusion of the systems confined between smooth and rough walls[52], they show that the adsorption behavior and the solvation pressure are significantly affected by the roughness of the confining surface[53] and that different liquid and solid phases that exist in the smooth confined are not present in the rough case[44].

In this work we address the question of which are the effects of the roughness of the nanopore wall in the physical properties of an anomalous fluids. Our analysis is done in the

framework of an effective model that incorporates not only the two length scales traditionally present in the CS potentials but additional length scales representing the third coordination shell of the fluid. Our goal is also to understand the effect of the structure of the liquid in the thermodynamic, dynamic and structural properties of a fluid confined in a nanopore.

The paper is organized as follows: in Sec. II we introduce the model and the methods and simulation details are described; the results are given in Sec. III; and conclusions are presented in Sec. IV.

II. THE MODEL AND SIMULATION DETAILS

In this paper all physical quantities are computed in the standard LJ units[54],

$$r^* \equiv \frac{r}{r_0}\,, \quad \rho^* \equiv \rho r_0^3\,, \quad \text{and} \quad t^* \equiv t\left(\frac{\gamma}{m r_0^2}\right)^{1/2}\,, \tag{1}$$

for distance, density of particles and time , respectively, and

$$p^* \equiv \frac{p r_0^3}{\gamma} \quad U^* \equiv \frac{U}{\gamma} \quad \text{and} \quad T^* \equiv \frac{k_B T}{\gamma} \tag{2}$$

for the pressure, energy and temperature, respectively, where $r_0 = 2.869$ Å is the distance parameter, $\gamma = 0.30$ kcal/mol the energy parameter and m the mass of each particle. Since all physical quantities are defined in reduced LJ units, the * is omitted, in order to simplify the discussion.

The fluid is composed by N spherical particles of diameter $\sigma = 1.47$ and mass m confined between two parallel and fixed plates. We have studied two kinds of nanopores: with smooth and structured walls. Smooth plates are modeled by force fields and do not have structure, interacting continuously with the fluid. Structured plates are formed by spherical particles in a square lattice with punctual interactions. A schematic depiction for the systems with (a) smooth and (b) structured plates is shown in Fig. 1.

The particles of the fluid interact through the isotropic effective potential[55] given by

$$\frac{U(r)}{\epsilon} = \left[\left(\frac{\sigma}{r}\right)^a - \left(\frac{\sigma}{r}\right)^b\right] + \sum_{j=1}^{4} h_j \exp\left[-\left(\frac{r - c_j}{w_j}\right)^2\right]\,, \tag{3}$$

with the parameters given in the Table I. Fig. 2 shows the potential versus distance in dimensionless units. In this work, we use $\epsilon/\gamma = 0.02$.

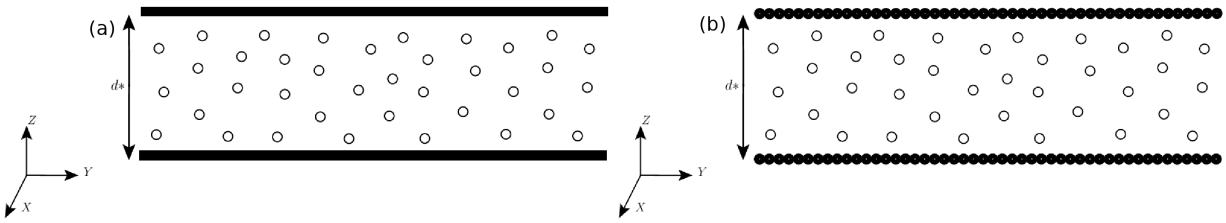

FIG. 1. Schematic depiction of the particles confined between (a) smooth and (b) structured plates.

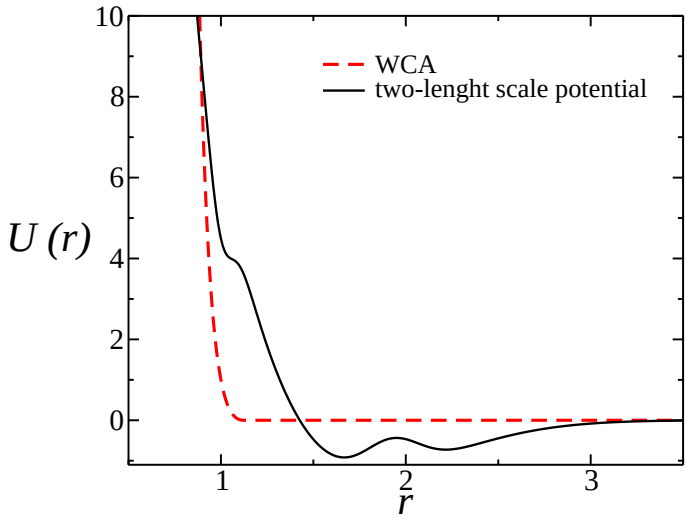

FIG. 2. Particle-particle interaction potential (black solid line) and particle-plate interaction potential (red dashed line).

This effective potential was derived from the Ornstein-Zernike and integral equations applied to the oxygen-oxygen radial distribution function of the atomistic model ST4[58]. At short distances it shows two characteristic length scales: one at $r_1 \approx 1.1$ and another at $r_2 \approx 1.6$, as in the usual coarse grained potentials proposed to model the anomalous liquids. In addition a third length scale at $r_3 \approx 2.2$ is also present. Since the derivation of the potential was based in the oxygen radial distribution function these length scales represent the oxygen-oxygen distances related to the relevant coordination shells in the liquid. The bulk system exhibits waterlike anomalies, and the liquid-gas and liquid-liquid critical points predicted for water[55].

In the confined system the particles of the fluid interact with the wall by the Weeks-

Chandler-Andersen (WCA) potential,

$$U(r) = \begin{cases} U_{\rm LJ}(r) - U_{\rm LJ}(r_{cw}), & r \leq r_{cw} \\ 0, \qquad r > r_{cw}\ , \end{cases} \tag{4}$$

where $U_{LJ}(r)$ is the standard 12-6 LJ potential[54]. The cutoff distance is $r_{cw} = 2^{1/6}$. For smooth plates, the interaction occurs just in z direction and the potential is written as $U_{LJ}(z)$.

TABLE I. Parameters of the particle-particle potentials in units of Å and kcal/mol.

Parameters	values	Parameters	values	Parameters	values	Parameters	values
a	9.065	w_1	0.253	h_1	0.5685	c_1	2.849
b	4.044	w_2	1.767	h_2	3.626	c_2	1.514
ϵ	0.006	w_3	2.363	h_3	−0.451	c_3	4.569
σ_p	4.218	w_4	0.614	h_4	0.230	c_4	5.518

The dynamic, thermodynamic and structural properties of the fluid was studied using molecular dynamics simulation in the NVT ensemble. The Nose-Hoover thermostat[56,57] was used to fix the temperature, with a coupling parameter $Q = 2$. The interaction potential between particles, Eq. (3), has a cutoff radius $r_c = 3.5$.

The fluid was confined by two different kinds of parallel walls: smooth and structured. The plates are fixed and are located each one at $z = 0$ and $z = d$. The smooth plates are modeled by force fields in z direction and have no structure. The interaction between smooth plates and the fluid was done using the WCA (Weeks-Chandler-Andersen) potential, like shown in Eq. 4, but considering just the z component. The structured plates are constructed by placing spherical particles of effective diameter σ in a square lattice of area L^2. The fluid-wall interaction also is given by a WCA potential.

In z direction the space occupied for the fluid was limited by the confining plates. Due the excluded volume between the fluid near to the plates, the distance d between them need to be corrected to an effective distance d_e, that can be approach by $d_e \approx d - \sigma$[59]. Consequently, the effective density will be $\rho = N/(d_e L^2)$.

Systems with plate separations $d = 2.5$, 4.2, 5.2 and 8.0 were analyzed. Several densities and temperatures were simulated to obtain the full phase diagrams for each case. For systems

with $d = 2.5$, 4.2 and 5.2 $N = 507$ particles were employed, while for $d = 8.0$ $N = 546$ particles were used. Two different initial configuration of the systems were simulated: solid and liquid states. Using different initial configurations allow us to identify precisely the final state of the system, avoiding metastability. The equilibrium state was reached after 4×10^5 steps, followed by 8×10^5 simulation run. We used a time step $\delta t = 0.001$, in reduced units, and all the physical quantities were get with 50 uncorrelated samples. To check the stability of the systems, we verify the energy as function of time and the perpendicular pressure and parallel pressure as function of density.

Since the fluid is confined in the z direction, the thermodynamic averages was calculated in components parallel and perpendicular to the plates[60]. The systems have periodic boundary conditions in x and y directions and they are extensive just in area and not in the distance between the plates.

The parallel pressure was calculated using the Virial expression for the x and y directions[59],

$$P_{\parallel} = \rho k_B T + \frac{1}{2V} \left\langle \mathcal{V}_{\parallel} \right\rangle , \tag{5}$$

where $\mathcal{V}_{\parallel}$ is given by

$$\mathcal{V}_{\parallel} = -\sum_{i=1} \sum_{j>i} \frac{x_{ij}^2 + y_{ij}^2}{r_{ij}} \left(\frac{\partial U(r)}{\partial r} \right)_{r=r_{ij}} . \tag{6}$$

The lateral diffusion coefficient, $D_{\parallel}$, was calculated using the mean square displacement (MSD), related from Einstein relation,

$$D_{\parallel} = \lim_{\tau \to \infty} \frac{\langle \Delta r_{\parallel}(\tau)^2 \rangle}{4\tau}, \tag{7}$$

where $r_{\parallel} = (x^2 + y^2)^{1/2}$ is the parallel distance of the particles.

The structure of the system was studied considering the lateral radial distribution function, $g_{\parallel}(r_{\parallel})$, calculated in specific slabs between the plates. The definition of the $g_{\parallel}(r_{\parallel})$ is usually given by

$$g_{\parallel}(r_{\parallel}) \equiv \frac{1}{\rho^2 V} \sum_{i \neq j} \delta(r - r_{ij}) \left[\theta \left(|z_i - z_j| \right) - \theta \left(|z_i - z_j| - \delta z \right) \right] . \tag{8}$$

The $\theta(x)$ is the Heaviside function and it restricts the sum of particle pairs in the same slab of thickness $\delta z = \sigma$. The $g_{\parallel}(r_{\parallel})$ is proportional to the probability of finding a particle at a distance $r_{\parallel}$ from a referent particle.

III. RESULTS

Thermodynamic, dynamic and structural behavior Smooth plates

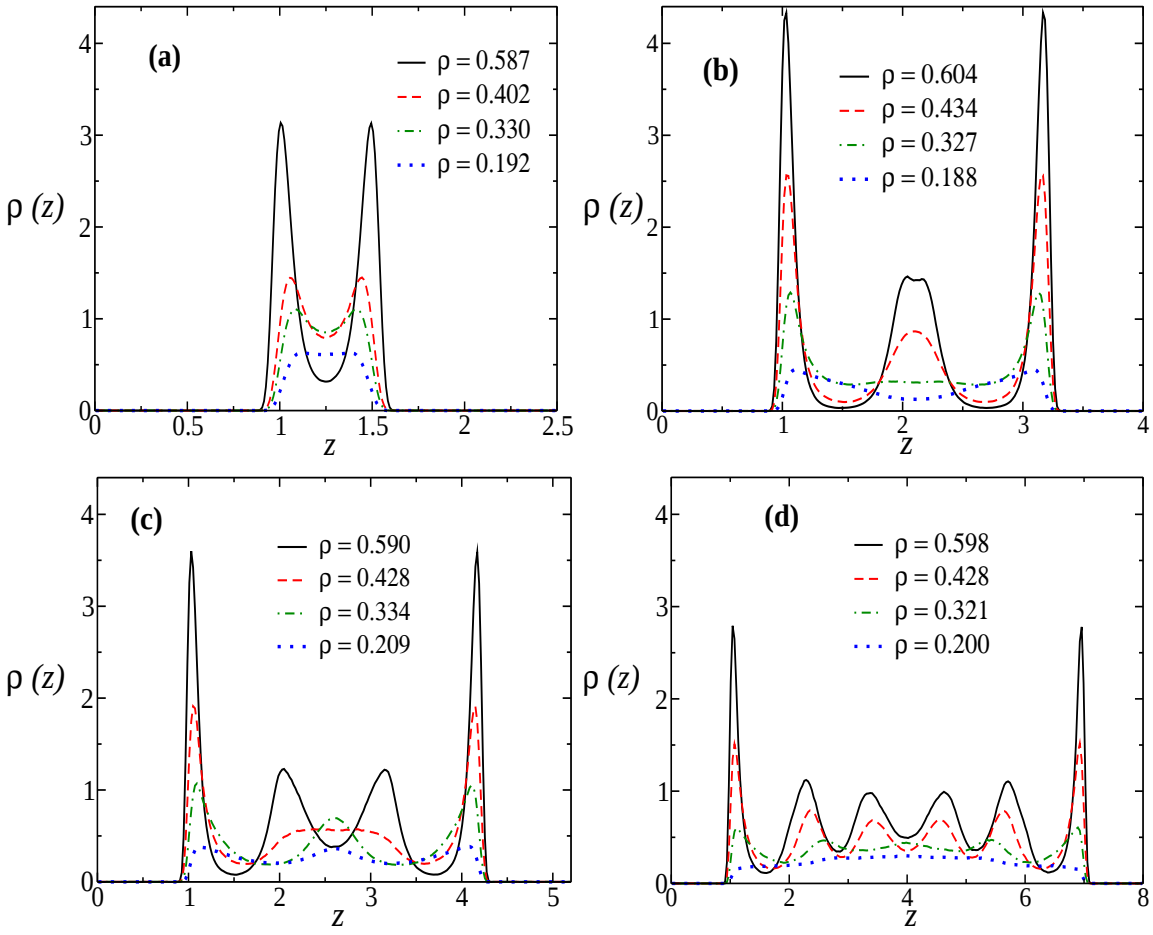

FIG. 3. Transversal density profiles for systems confined by smooth plates with $T = 0.80$ and different densities at (a) $d = 2.5$, (b))$d = 4.2$ (c)$d = 5.2$ and (c) $d = 8.0$.

A schematic depiction of the system confined by smooth plates is shown in the figure **??**(a). First, the effect of the structure of the liquid when confined by an uniform field is checked. Fig. 3 illustrates the transversal density profiles for plates separated at (a) $d = 2.5$,(b) $d = 4.2$ (c) $d = 5.2$ and (d) $d = 8.0$ at $T = 0.80$ and several densities. In all

cases the system form layers, however the number of layers is dependent on the degree of confinement and of the density of the systems, what is consistent with results for atomistic such as SPC/E[61] and coarse grained approximations with three body terms as mW[62] model.

For higher degrees of confinement, $d = 2.5$, the fluid is structured in one or two layers, depending on the density of the system. Fig. 3(a) shows that two layers are observed for high densities ($\rho = 0.587$), while one layer occurs for low densities ($\rho = 0.192$). The mechanism for the presence of different structures goes as follows. For low densities the wall does not induce correlations and layering at the z direction therefore one layer or bulk structure is formed. As the density becomes higher, the competition between particle-particle and wall-particle interactions leads to the formation of layers. There are two typical separations for the layers. The first is $r_3 - r_1 \approx 1.1$, which corresponds to the minimum of energy, and the second one is $r_2 - r_1 \approx 0.5$, which is the second lowest energy potential. Since the plate separation is $d = 2.5$, the confinement do not allow the fluid particles to remain in the first distance (minimum energy), and the layers separation is then equal to the second typical separation.

For other degrees of confinement, $d = 4.2, 5.2, 8.0$, the same competition between wall-particle and particle-particle interactions appears as shown in the Fig. 3. For low densities an uniform distribution with just one layer appears and as the density increases, two, three, four or even five layers are present. However, since in this case the plates are further apart, the interlayer distance is is $r_3 - r_1 \approx 1.1$ that corresponds to the distance between the shoulder length scale and the third coordination shell in the Figure **??**.

The diffusion anomaly observed in liquid water is characterized by the increase of the diffusion coefficient of the fluid when the pressure, or density, increases. For normal fluids, this coefficient decreases when the fluid is compressed. The Fig. 4 shows the lateral diffusion coefficient ($D_{\parallel}$) as function of density of the system for (a) $d = 2.5$, (b) $d = 4.2$, (c) $d = 5.2$ and (d) $d = 8.0$. The range in temperature and density for which the anomaly in diffusion is the same for the distances $d = 4.2, 5.2, 8.0$ but is different at $d = 2.5$. These two behaviors, one at $d = 2.5$ and another at larger distances might be related with the different length scales involved in the close and larger distances as observed in the Figure 3.

In addition to the anomalous dynamic properties of the confined liquid, the thermodynamic and phase space were also explored. The system with $d = 2.5$ illustrated in the Fig. 5 (a) shows the presence of a Temperature of Maximum Density, TMD, as a solid line, a vapor

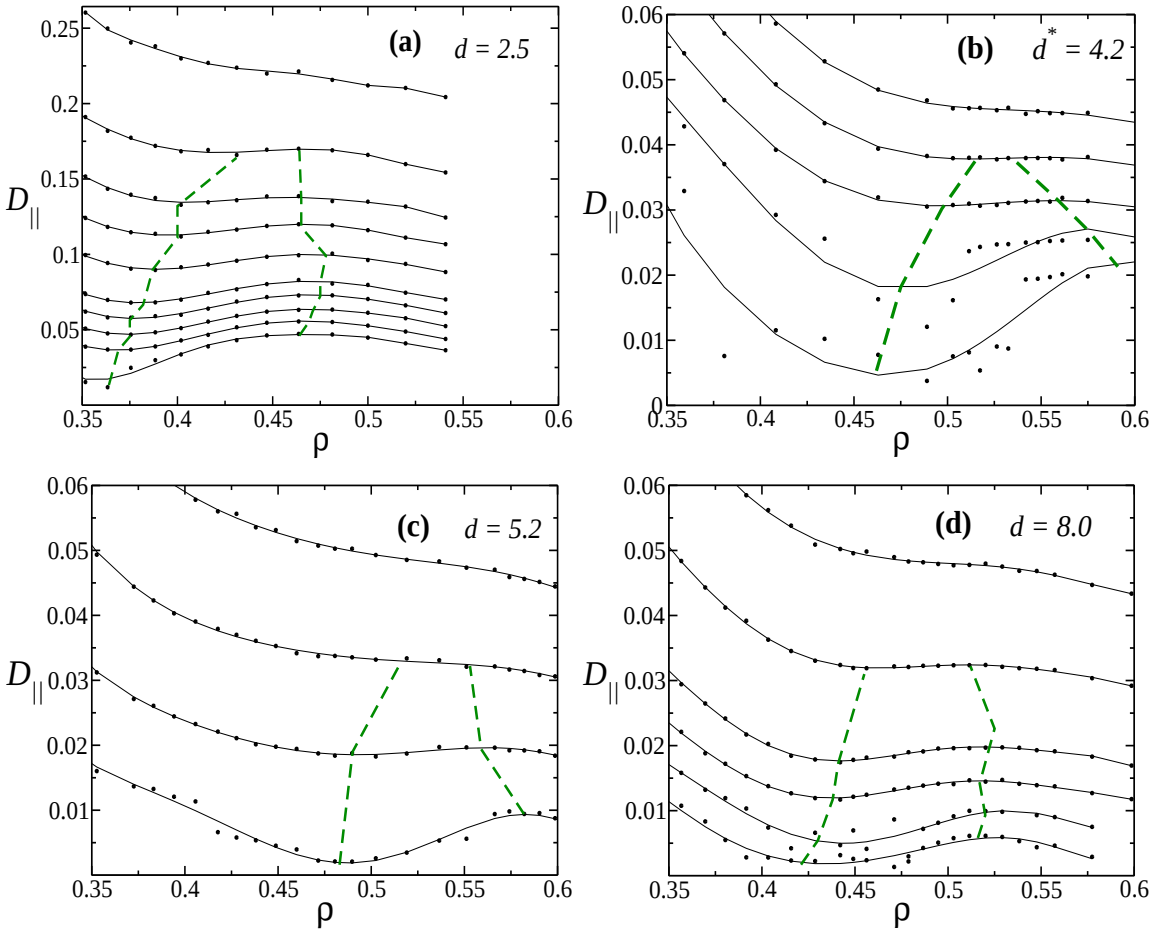

FIG. 4. Diffusion coefficient as function of density for (a) $d = 2.5$ and isotherms 0.60, 0.65, 0.70, 0.75, 0.80, 0.90, 1.00, 1.10, 1.25 and 1.50, (b) $d = 4.2$ and isotherms 0.60, 0.65, 0.70, 0.75 and 0.80, (c) $d = 5.2$ and isotherms 0.50, 0.60, 0.70 and 0.80 and (d) $d = 8.0$ and isotherms 0.45, 0.50, 0.55, 0.60, 0.70 and 0.80. The dots are the simulated data and the black solid lines are polinomial fits. The dashed green lines bound the region where the diffusion are anomalous.

phase and two liquid phases. This system, therefore, exhibits two stable critical points: a vapor-liquid critical point, VLCP, at $P_c = 0.08$ and $T_c = 0.55$ (red circle) and a liquid-liquid critical point, $LLCP$, at $P_c = 4.0$ and $T_c = 0.3$ (blue square). In the bulk system the $VLCP$ occurs at $P_c = 0.078$ and $T_c = 1.98$ while the $LLCP$ appears at $P_c = 1.86$ and $T_c = 0.48$. The comparison between the confined and the bulk systems indicates that the VLCP was shifted to lower temperatures, but did not present significantly changes in pressure. Meanwhile, the $LLCP$ is shifted to lower temperatures and higher pressures in relation to bulk, what is in agreement with results obtained for theoretical models involving anomalous fluids[63] and TIP4P water[64]. The dashed lines in the Fig. 5 (a) represent the diffusion extremes and the

pointed line indicates the limit between amorphous and fluid phases. The shifting of the critical point to lower temperatures can be assumed as a natural effect of the confinement, since the nanopore walls increase the entropy of the free energy of the system, favoring the disordered fluid phase. The increase in the pressure for the appearance of the $LLCP$ is the result of the layering imposed by the walls. The layering allows for a high density interlayer making the full high density liquid only to appear at high densities.

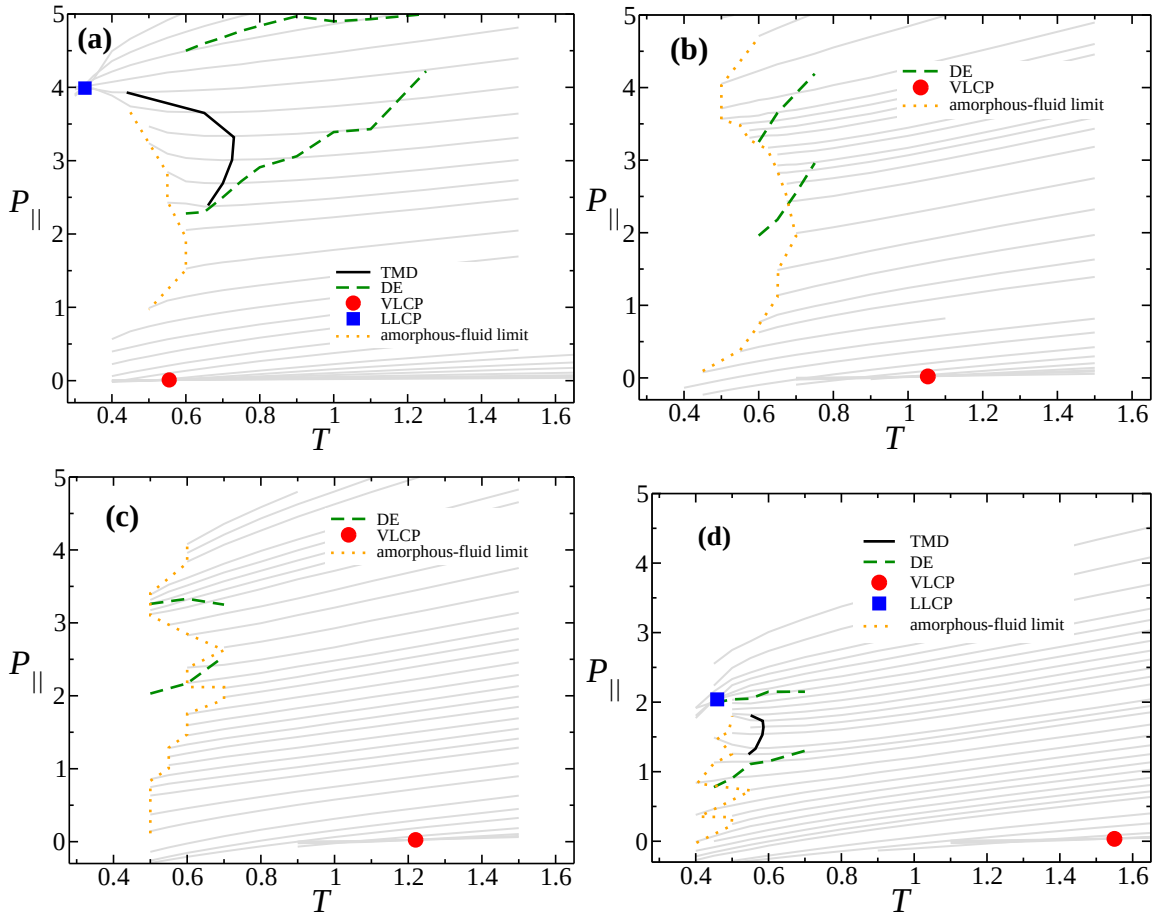

FIG. 5. Parallel pressure versus temperature phase diagram for systems with smooth plates separated by distances (a) $d = 2.5$, (b) $d = 4.2$, (c) $d = 5.2$ and (d) $d = 8.0$. The thin lines represent different isochores.

For the plates separations $d = 4.2$ and 5.2, the phase diagrams illustrated in the Fig. 5 (b) and (c) show the presence of a VLCP also shifted to lower temperatures when compared with the bulk system. However, the TMD line and the $LLCP$ could not be determined.

Due to the increase of the entropic effects for a system under confinement the melting line and the $LLCP$ should in principle move to lower temperatures. Whereas, we observed that

the melting temperatures (T_m) for the confined systems are higher than the bulk system. In addition the change in the value of T_m is not monotonic with d similarly with what is observed in atomistic[29] and waterlike fluids[41].

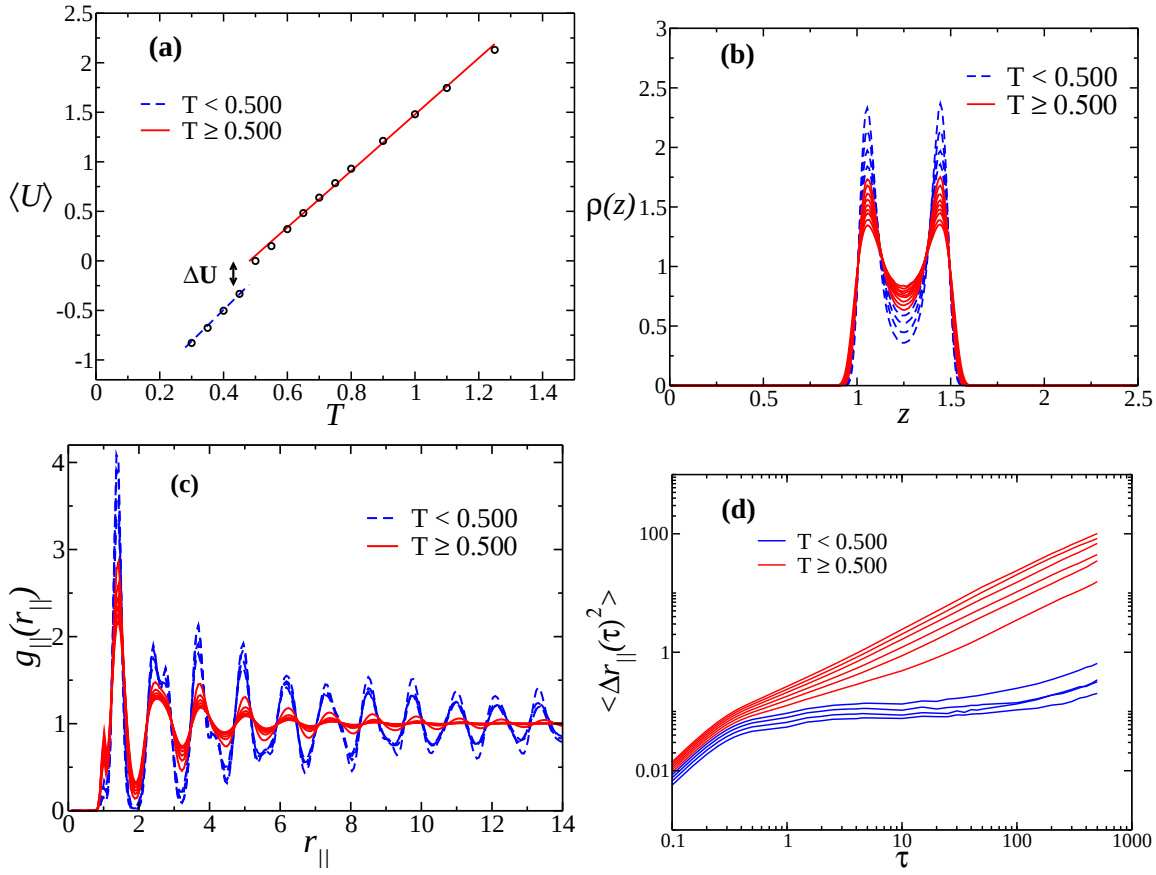

FIG. 6. System with plates separated at $d = 2.5$ and density $\rho = 0.402$. In (a), the mean potential energy as function of temperature, in (b) the transversal density profile, in (c) the lateral radial distribution function ($g_{||}(r_{||})$) for the contact layer and in (d) the mean square displacement in lateral direction.

In order to understand why the melting line moves to higher temperatures, covering the TMD and the $LLCP$, the structure in this region was analyzed. For this purpose, the transition is analyzed for $d = 2.5$ and $d = 5.2$. Fig. 6 in (a) illustrates the mean potential energy as function of temperature, in (b) shows the transversal density profile, in (c) plots the lateral radial distribution function ($g_{||}(r_{||})$) for the contact layer and in (d) presents the mean square displacement in lateral direction for $d = 2.5$ and $\rho = 0.536$. We observe clearly a first order phase transition between an amorphous solid and a liquid phases. A discontinuous behavior was detected at $T = 0.50$. For $T < 0.50$, the energies have lower

values, the density profiles and the $g_{||}(r_{||})$ have a well defined structure and the $\langle \Delta r^2(t) \rangle$ has a small inclination, showing a typical behavior of an amorphous solid phase. Whereas, for $T \geq 0.500$, the energy shows high values and the density profiles, the $g_{||}(r_{||})$ and the $\langle \Delta r^2(t) \rangle$ present a characteristic behavior of liquid phase. Amorphous solid-liquid first order phase transition was already observed for TIP5P model confined between smooth hydrophobic plates[65]. The density profile shown in Figure. 6(b) , however, indicates that amorphous solid phase is not structured inside each layer but is present in the space between layers.

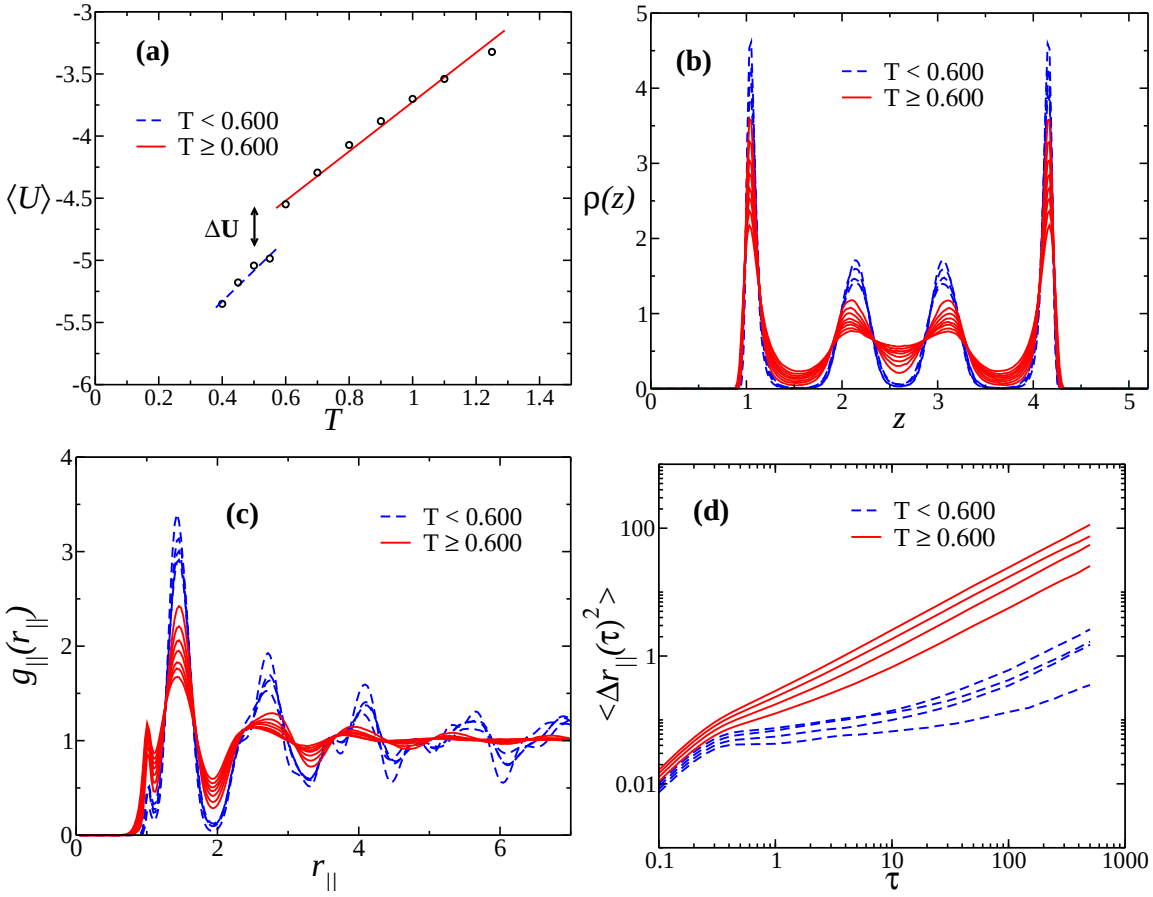

FIG. 7. System with plates separated at $d = 5.2$ and density $\rho = 0.536$. In (a), the mean potential energy as function of temperature, in (b) the transversal density profile, in (c) the lateral radial distribution function ($g_{||}(r_{||})$) for the contact layer and in (d) the mean square displacement in lateral direction.

In the case of $d = 5.2$ illustrated in the Figures 7 the first order transition is observed at $T = 0.06$ because at this temperature the energy has a jump in (a), the radial distribution function shows a change in the structure from liquid to amorphous solid in (c) and the mean

square displacement changes from non zero to zero diffusion in (d). The density profile illustrated in the Figures 7 (b) differently than what is observed for $d = 2.5$ shows that the amorphous solid structure is confined to a single layer.

The different ways in which the amorphous solid structures accommodates for the cases $d = 2.5$ and $d = 5.2$ under confinement explains the non monotonic behavior of the melting temperature. While for strong confinement the amorphous solid forms across the layers in the region $d = 5.2$ (and also $d = 4.2$) the amorphous solid structure is confined to a single layer. As the distance increases further the amorphous solid are again formed across layers approaching the bulk structure.

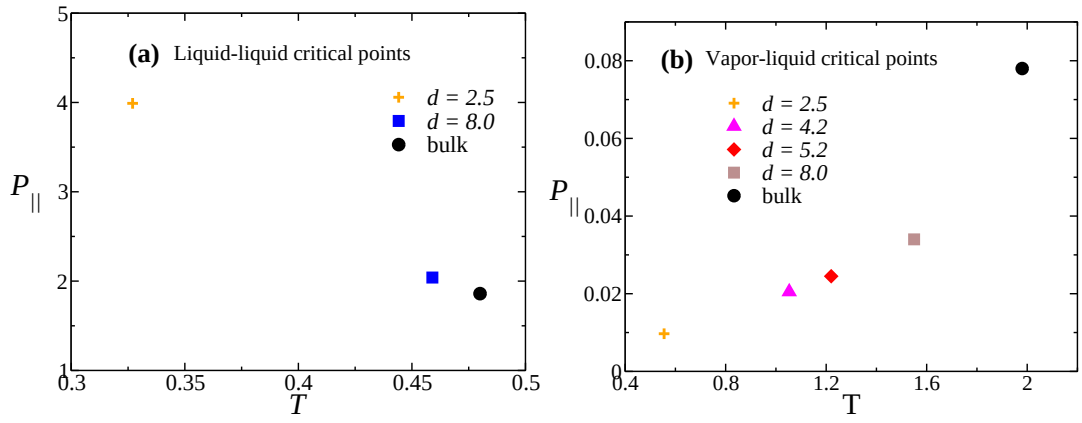

FIG. 8. Location of (a) $LLCP$ and (b) $VLCP$ for all the distances between the smooth plates.

The effects of the confinement in the critical points of water are dependent on the geometry and wall structure of confinement that are being considered. For example, when the water is confined in the pore matrix[64], the $LLCP$ and the TMD line are shifted to lower temperatures and higher pressures in relation to bulk. But, in aqueous solutions of NaCl, Corradini and Gallo[66] shows that the increase of salt concentration in water (TIP4P) shifts the $LLCP$ to higher temperatures and lower pressures in relation to bulk. Our results for the $LLCP$ and $VLCP$ are summarized in Fig. 8 and are in good agreement with the results for the pore media[64]. This suggests that the salt/water long-range order interaction leads to changes in the water phase behavior what is not present in the short-range wall-particle interaction modeled by our system.

Experimental results show a non-monotonic behavior for the melting line and a strong dependence with the quality of the nanopore walls[29] what is observed in our results. In the next section we will exam how the structure of the plates also have important effect in the

solidification of the system and in the location of the anomalies and critical points.

Structured plates

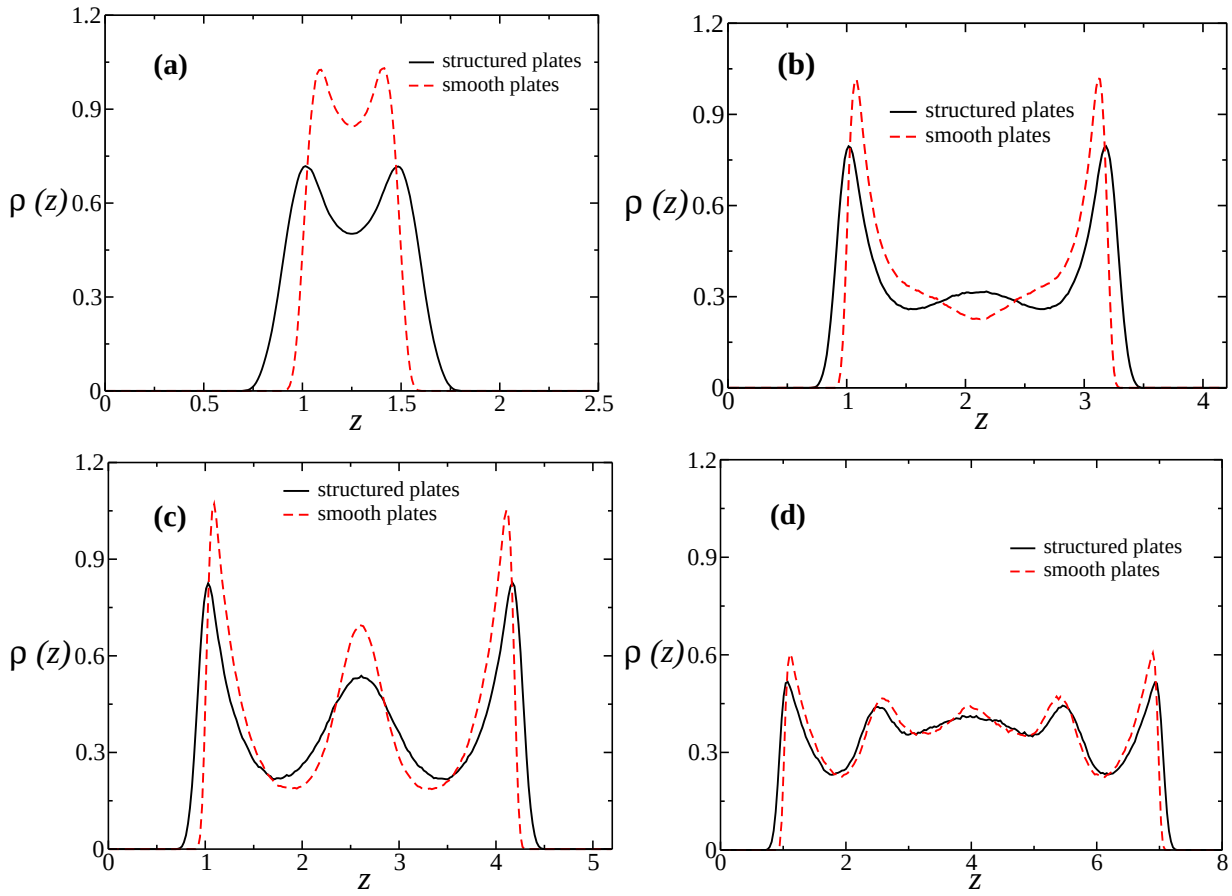

FIG. 9. Comparison of transversal density profile for systems confined by structured and smooth plates at $T = 0.80$ and different densities at (a) $d = 2.5$, (b) $d = 5.2$ and (c) $d = 8.0$. The confinement at $d = 4.2$ is not shown for simplicity.

The second scenario we address here is the effect of the structure in the wall has in the thermodynamic and dynamical behavior of the confined liquid. In this case, the plates are constructed by spherical particles in a square lattice, as sketched in Fig. **??** (b). The interaction potential between fluid particles and walls particles is given by the WCA potential (Eq. 4). A layering structure similar to picture observed for smooth plates analyzed in previous section is also present for structured plates. In Fig. 9 the transversal density profiles for smooth and structured plates are compared for: (a) for $d = 2.5$ and $\rho = 0.310$, (b) for $d = 5.2$ and $\rho = 0.334$ and (c) for $d = 8.0$ and $\rho = 0.321$. In all these cases the

temperature is the same, $T = 0.80$. As the nanopore width decreases, the difference in the layer structure between the smooth and the structured walls increases. For $d = 8.0$, the fluid exhibits almost the same density profile for the two types of confinement. This shows that for confined systems the fluid density profile is affected by the nanopore structure, particularly for strongly confined systems.

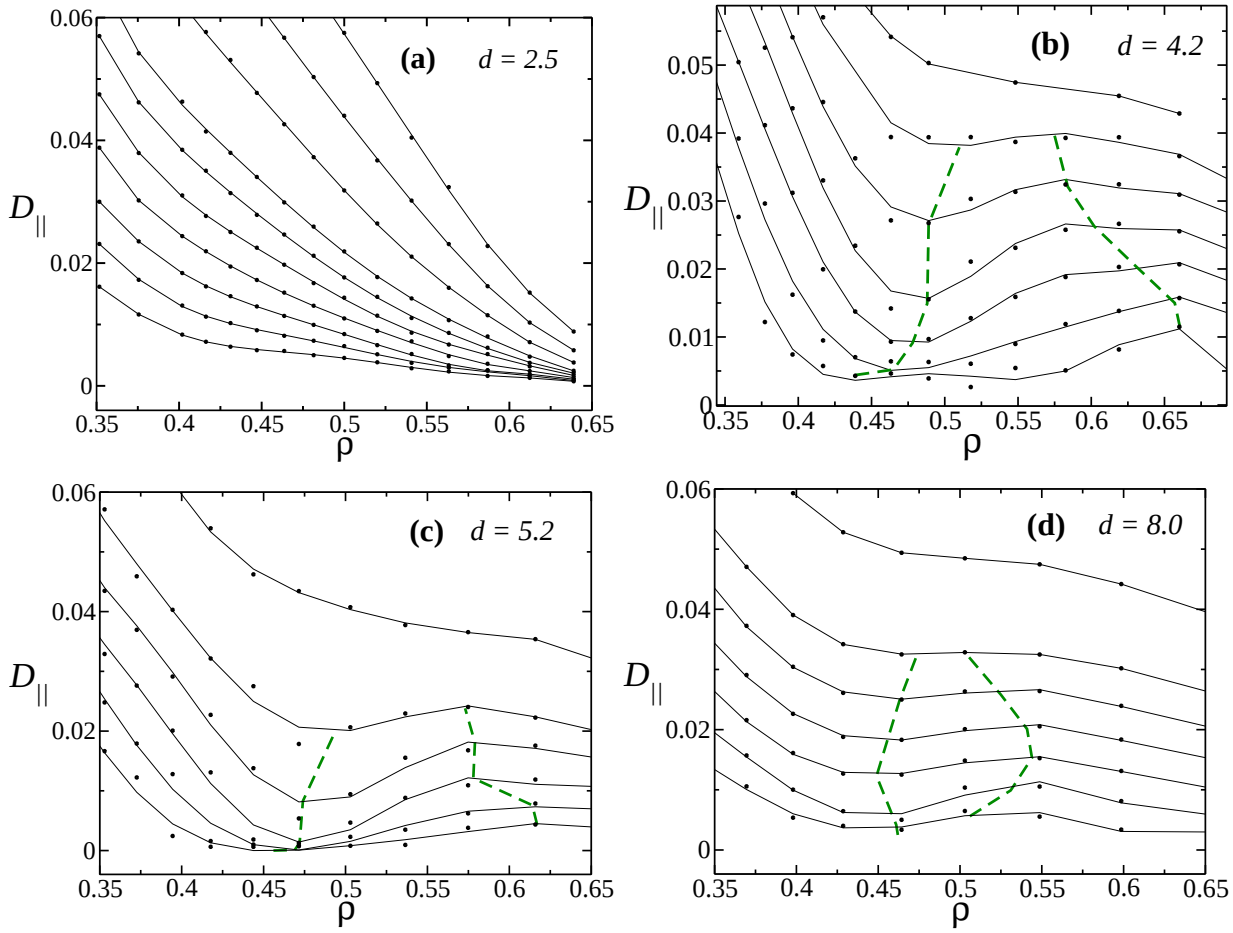

FIG. 10. Diffusion coefficient as function of density for (a) $d = 2.5$ and isotherms 0.50, 0.55, 0.60, 0.65, 0.70, 0.75, 0.80, 0.90, 1.00 and 1.10, (b) $d = 4.2$ and isotherms 0.60, 0.65, 0.70, 0.75, 0.80, 0.85 and 0.90, (c) $d = 5.2$ and isotherms 0.50, 0.55, 0.60, 0.65, 0.70 and 0.80 and (c) $d = 8.0$ and isotherms 0.45, 0.50, 0.55, 0.60, 0.65, 0.70 and 0.80. The dots are the simulated data and the black solid lines are polynomial fits. The dashed green lines bound the region where the diffusion are anomalous.

Another property of the liquid in which the structure of the confining surface might matter is the diffusion. Fig. 10 illustrates the diffusion coefficient in the parallel direction to the plates as function of the fluid density, for nanopores with size $d = 2.5$, $d = 4.2$, $d = 5.2$ and

$d = 8.0$. The diffusion anomaly was observed for systems with plates separated at $d = 4.2$, $d = 5.2$ and $d = 8.0$, while for $d = 2.5$ no anomalous behavior was detected in the range of temperatures studied – at low temperatures the fluid presents solidification, lead mainly by the nanopore structure.

Comparing the dynamical behavior of the systems, we verify that the fluid confined between structured plates behaves completely different from the smooth cases, particularly for small values of d. For $d = 2.5$, systems confined by smooth plates shows a large region of pressures and temperatures in which the diffusion anomaly is present (Fig. 4), while for structured walls, the fluid dynamically behaves like normal systems, without diffusion anomaly for the range of temperatures studied. The reason for this difference is that the structure of the wall plays a very important role in the structure of the liquid close to the wall and since at $d = 2.5$ the liquid is closer to the wall when compared with the smooth plates, the structure the wall determines the arrangement of the liquid. The liquid particles will be able to occupy the space between the wall particles.

The parallel pressure versus temperature phase diagrams are shown in the Fig. 11 for (a) $d = 2.5$, (b) $d = 5.2$, (c) $d = 4.2$ and (d) $d = 8.0$. The lines in the graph go as follows: the TMD lines for each case is represented by solid lines, the diffusion extremes by dashed lines, the $VLCP$ by squares, the $LLCP$ by circles and the limit between fluid and amorphous solid phases by dotted lines.

For structured nanopores with $d = 2.5$, the density and diffusion anomalies and the $LLCP$ are not observed outside the amorphous regions. This is an effect of the influence of the wall-water potential that favors particles close to the wall to occupy the spaces between wall particles. Then the particle-particle two length scales competition that leads to the presence of density and diffusion anomalies does not happen, instead there is a competition between particle-particle and wall-particle interactions. The solidification for the system in this case is similar to what happens in the last section for $d = 4.2$, $d = 5.2$ and $d = 8$. In this case, however, the melting temperatures are lower than in the smooth potential case. The competition between the wall-particle interaction that favors one solid arrangement with the particle-particle interaction that favor other arrangement explains the difference between the melting for rough and smooth walls. Classical water model TIP5P confined between structured hydrophobic plates also presents a shift for higher temperatures[67].

The Fig. 12 summarizes the behavior of (a) $LLCP$ and (b) $VLCP$ for the different

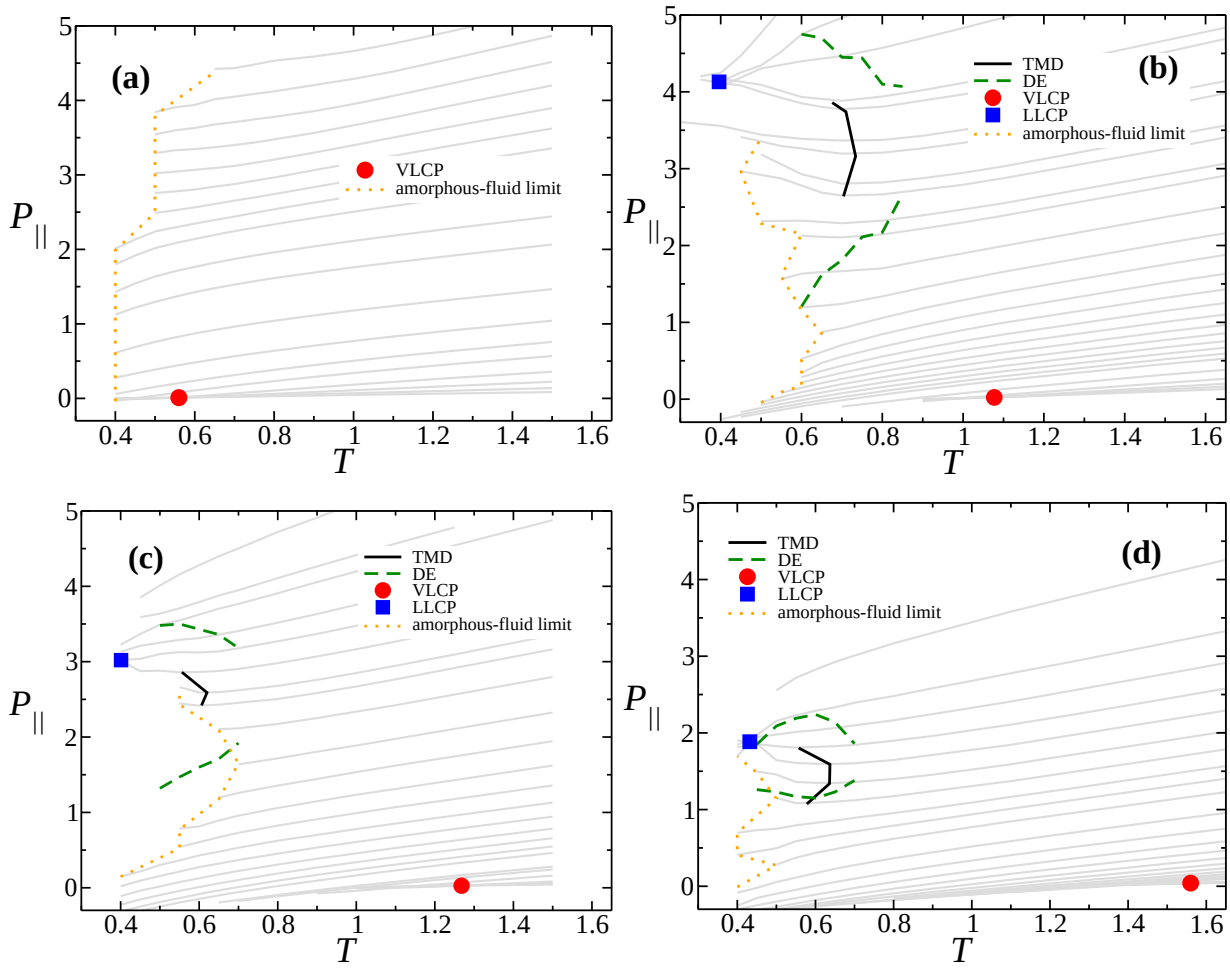

FIG. 11. Parallel pressure versus temperature phase diagram for systems with structured plates separated by distances (a) $d = 2.5$, (b) $d = 4.2$, (c) $d = 5.2$ and (c) $d = 8.0$. The thin lines represents

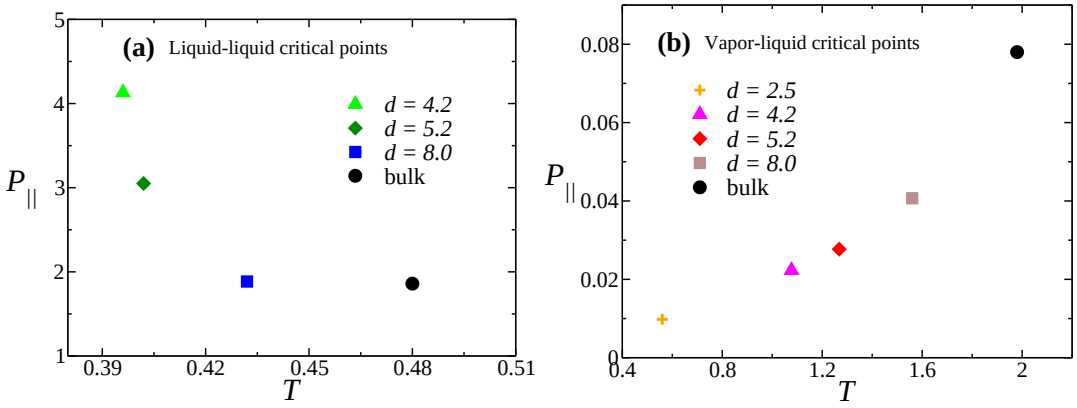

FIG. 12. Location of (a) $LLCP$ and (b) $VLCP$ for all the distances between the structured plates.

nanopores sizes and structured walls. The location of both critical points changes with the

distances between the plates. As the nanopore width d decreases, the $LLCP$ goes to lower temperatures and higher pressures, while the $VLCP$ is shifted to lower temperatures and lower pressures too.

IV. CONCLUSIONS

In this work we have studied the effects of the nanopore structure and of the water potential length scales in the waterlike properties of an anomalous fluid. First, we tested the effect of using a three length scales potential for analyzing the fluid behavior. In this case the system confined by very small distances exhibits a different behavior when compared with confinement by intermediate and large distances. This difference can be explained by the the arrangement of the fluid particles in the first, second or third length scale of the potential. Then we check the differences in the thermodynamic and dynamic anomalies of the fluid when it was confined between smooth and structured walls. When observed, the density and diffusion anomalies are shifted to lower temperatures and higher pressures in relation to bulk for both kinds of confinement. However, the critical points and the limit between solid and fluid phases present a significant difference for each system. For high degrees of confinement the properties of the fluid is very well defined when confined by smooth nanopores, but the fluid crystallizes for structured walls and small d. For intermediates separation of walls, smooth confinement present solidification and structured confinement do not. So, a non-monotonic behavior is observed in the properties of the fluid with d when confined by smooth plates and a monotonic behavior with d when confined between structured plates. The scales of the fluid-fluid and the fluid-plate interaction potential are responsible for the different behavior observed for each kind of confinement.

ACKNOWLEDGMENTS

We thank for financial support the Brazilian science agencies, CNPq and Capes. This work is partially supported by CNPq, INCT-FCx.

* leandro.krott@ufrgs.br

† josebordin@unipampa.edu.br

‡ ney.barraz@uffs.edu.br

§ marciabarbosa@ufrgs.br

[1] M. Chaplin, Seventy two anomalous properties of water, `www1.lsbu.ac.uk/water/water_anomalies.html`, 2015.

[2] R. Waler, *Essays of natural experiments*, Johnson Reprint, New York, 1964.

[3] G. S. Kell, J. Chem. Eng. Data **20**, 97 (1975).

[4] C. A. Angell, E. D. Finch, L. A. Woolf, and P. Bach, J. Chem. Phys. **65**, 3063 (1976).

[5] P. H. Poole, F. Sciortino, U. Essmann, and H. E. Stanley, Nature (London) **360**, 324 (1992).

[6] Y. Liu, J. C. Palmer, A. Z. Panagiotopoulos, and P. G. Debenedetti, J. Chem. Phys. **137**, 214505 (2012).

[7] J. C. Palmer et al., Nature **510**, 385âĂŞ388 (2014).

[8] A. Taschin, P. Bartolini, R. Eramo, E. Righini, and R. Torre, Nature communications **4**, 2401 (2013).

[9] I. Brovchenko, A. Geiger, and A. Oleinikova, J. Chem. Phys. **123**, 044515 (2005).

[10] P. H. Poole, S. R. Becker, F. Sciortino, and F. W. Starr, J. Phys. Chem. B **115**, 14176 (2011).

[11] P. H. Poole, R. K. Bowles, I. Saika-Voivod, and F. Sciortino, J. Chem. Phys. **138**, 034505 (2013).

[12] A. Kesselring et al., J. Chem. Phys. **138**, 244506 (2013).

[13] F. W. Starr, Nature Physics **10**, 628 (2014).

[14] T. Yagasaki, M. Matsumoto, and H. Tanaka, Phys. Rev. Lett. **89**, 02030 (2014).

[15] T. Morishite, Phys. Rev. Lett. **87**, 4659 (2001).

[16] I. Saika-Voivod, F. Sciortino, and P. Poole, Phys. Rev. E **63**, 011202 (2001).

[17] E. Lascaris, M. Hemmati, S. V. Buldyrev, H. E. Stanley, and C. A. Angell, J. Chem. Phys. **140**, 224502 (2014).

[18] V. V. Vasisht, S. Saw, and S. Sastry, Nature Phys. **7**, 549 (2011).

[19] J. N. Glosli and F. H. Ree, Phys. Rev. Lett. **82**, 4659 (1999).

[20] S. Scandolo, Proc. Natl Acad. Sci. USA **100**, 3051 (2003).

[21] F. Smallenburg, L. Filion, and F. Sciortino, Nature Phys. **10**, 653 (2014).

[22] D. T. Limmer and D. Chandler, J. Chem. Phys. **135**, 135503 (2011).

[23] D. T. Limmer and D. Chandler, J. Chem. Phys. **138**, 214504 (2013).

[24] C. A. Angell, On the uncertain distinction between fast landscape exploration and secondamorphous phase (ideal glass) interpretations of the ultrastable glass phenomenon, J. Non-Cryst. Solids. http://dx.doi.org/10.1016/j.jnoncrysol.2014.08.044, 2014.

[25] L. Liu, S.-H. Chen, A. Faraone, S.-W. Yen, and C.-Y. Mou, Phys. Rev. Lett. **95**, 117802 (2005).

[26] A. Nagoe, S. Iwaki, M. Oguni, and K. Tôzaki, J. Phys. Soc. Jpn. **83**, 094601 (2014).

[27] F. Mallamace et al., J. Chem. Phys. **141**, 18C504 (2014).

[28] S. Jähnert et al., Phys. Chem. Chem. Phys. **10**, 6039 (2008).

[29] J. Deschamps, F. Audonnet, N. Brodie-Linder, M. Schoeffel, and C. Alba-Simionesco, Phys. Chem. Chem. Phys. **12**, 1440 (2010).

[30] M. Erko, N. Cade, A. G. Michette, G. H. Findenegg, and O. Paris, Phys. Rev. B **84**, 104205 (2011).

[31] K. Morishige and K. Kawano, J. Chem. Phys. **110**, 4867 (1999).

[32] D. W. Hwang, C.-C. Chu, A. K. Sinha, and L.-P. Hwang, J. Chem. Phys. **126**, 044702 (2007).

[33] S. Kittaka, K. Sou, T. Yamaguchi, and K. Tozaki, Phys. Chem. Chem. Phys **11**, 8538 (2009).

[34] A. Faraone, K.-H. Liu, C.-Y. Mou, Y. Zhang, and S.-H. Chen, Nature **130**, 134512 (2009).

[35] P. C. Hemmer and G. Stell, Phys. Rev. Lett. **24**, 1284 (1970).

[36] E. A. Jagla, Phys. Rev. E **58**, 1478 (1998).

[37] L. Xu et al., Proc. Natl. Acad. Sci. USA **102**, 16558 (2005).

[38] A. B. de Oliveira, P. A. Netz, T. Colla, and M. C. Barbosa, J. Chem. Phys. **124**, 084505 (2006).

[39] E. Lomba, N. G. Almarza, C. Martin, and C. McBride, J. Chem. Phys. **126**, 244510 (2007).

[40] J. da Silva, E. Salcedo, A. B. Oliveira, and M. C. Barbosa, J. Phys. Chem. **133**, 244506 (2010).

[41] L. Krott and M. C. Barbosa, J. Chem. Phys. **138**, 084505 (2013).

[42] L. B. Krott and M. C. Barbosa, Phys. Rev. E **89**, 012110 (2014).

[43] L. B. Krott and J. R. Bordin, J. Chem. Phys. **139**, 154502 (2013).

[44] J. R. Bordin, L. B. Krott, and M. C. Barbosa, J. Phys. Chem. C **118**, 9497 (2014).

[45] J. R. Bordin, L. B. Krott, and M. C. Barbosa, J. Chem. Phys. **141**, 144502 (2014).

[46] L. B. Krott, J. R. Bordin, and M. C. Barbosa, J. Phys. Chem. B **119**, 291 (2015).

[47] J. R. Bordin, A. B. de Oliveira, A. Diehl, and M. C. Barbosa, J. Chem. Phys **137**, 084504 (2012).

[48] J. R. Bordin, A. Diehl, and M. C. Barbosa, J. Phys. Chem. B **117**, 7047 (2013).

[49] J. R. Bordin, J. S. Andrade Jr., A. Diehl, and M. C. Barbosa, J. Chem. Phys. **140**, 194504 (2014).

[50] H. Holzmann, R. Ludwig, A. Geiger, and D. Paschek, Angewandte Chemie International Edition **46** (2007).

[51] O. Mishima, J. Chem. Phys. **133**, 144503 (2010).

[52] W. P. . Krekelberg, V. K. Shen, J. R. Errington, and T. M. Truskett, J. Chem. Phys. **135**, 154502 (2011).

[53] K. Yang, Y. Lin, X. Lu, and A. V. Neimark, J. Coll. Interf. Science **362**, 382 (2011).

[54] P. Allen and D. J. Tildesley, *Computer Simulation of Liquids*, Oxford University Press, Oxford, 1987.

[55] N. Barraz Jr., E. Salcedo, and M. Barbosa, J. Chem. Phys. **131**, 094504 (2009).

[56] W. G. Hoover, Phys. Rev. A **31**, 1695 (1985).

[57] W. G. Hoover, Phys. Rev. A **34**, 2499 (1986).

[58] T. Head-Gordon and F. H. Stillinger, J. Chem. Phys. **98**, 3313 (1993).

[59] P. Kumar, S. V. Buldyrev, F. W. Starr, N. Giovambattista, and H. E. Stanley, Phys. Rev. E **72**, 051503 (2005).

[60] M. Meyer and H. E. Stanley, J. Phys. Chem. B **103**, 9728 (1999).

[61] N. Giovambattista, P. J. Rossky, and P. G. Debenedetti, J. Phys. Chem. B **113**, 13723 (2009).

[62] E. B. Moore, J. T. Allen, and V. Molinero, J. Phys. Chem. C **116**, 7507 (2012).

[63] T. M. Truskett, P. G. Debenedetti, and S. Torquato, J. Chem. Phys. **114**, 2401 (2001).

[64] E. G. Strekalova et al., Journal of Biological Physics **38**, 97 (2012).

[65] S. Han, M. Y. Choi, P. Kumar, and H. E. Stanley, Nature Phys. **6**, 685 (2010).

[66] D. Corradini and P. Gallo, J. Phys. Chem. B **115**, 14161 (2011).

[67] R. Zangi, J. Phys.: Condens. Matter **16**, S5371 (2004).